Wearable EBG-Backed Belt Antenna for Smart On-Body Applications

Rui Pei, Mark Paul Leach, Eng Gee Lim, *Senior Member, IEEE*, Zhao Wang, Chaoyun Song, *Member, IEEE*, Jingchen Wang, Wenzhang Zhang, Zhenzhen Jiang, and Yi Huang, *Senior Member, IEEE*

***Abstract*—This article presents an innovative belt antenna with an electromagnetic band-gap (EBG) ground plane made of textile materials. The antenna can be applied in a smart belt system to set up a communication link with other electronic devices and/or host a variety of sensors to track human motions. The proposed belt antenna works at 2.45 GHz in the industrial, scientific, and medical radio band for Bluetooth low energy communications. Considering the effect the human body would have on the performance of a belt antenna, a textile ground plane is designed to be integrated into the trouser fabric behind the belt to provide isolation from the body and simultaneously improve antenna radiation characteristics. Through the application of the ground plane, the belt antenna achieves a maximum realized gain of 7.94 dBi and a minimum specific absorption rate of 0.04 W/kg at 0.5 W input power. During the design process, characteristic mode analysis is used to explore the underlining principle and further optimize the antenna performance. Two typical EBG structures are analyzed in detail for this application scenario. The suspended transmission line method is used to evaluate EBG performance variations when the textile ground plane is bent. A prototype of such a system is fabricated and tested. Experimental results shows that the belt antenna, together with the textile EBG ground plane, is an excellent candidate for a smart belt system with desirable radiation pattern, efficiency, and safety limit.**

***Index Terms*—Artificial magnetic conductor (AMC), belt antenna, characteristic mode analysis (CMA), electromagnetic band-gap (EBG) materials, metamaterial, specific absorption rate (SAR), wearable antennas.**

Manuscript received November 19, 2019; revised January 19, 2020 and February 16, 2020; accepted March 9, 2020. Date of publication March 30, 2020; date of current version July 29, 2020. This work was supported in part by the Xi'an Jiaotong Liverpool University Research Development Fund under Grant PGRS-13-03-06, Grant RDF-14-03-24, and Grant RDF-14-02-48 and in part by the Artificial Intelligence University Research Centre through Key Program Special Fund under Grant KSF-P-02. Paper no. TII-19-5032. *(Corresponding author: Mark Paul Leach.)*

Rui Pei, Mark Paul Leach, Eng Gee Lim, Zhao Wang, Jingchen Wang, and Zhenzhen Jiang are with the Department of Electrical and Electronics Engineering, Xi'an Jiaotong Liverpool University, Suzhou 215123, China (e-mail: rui.pei@xjtlu.edu.cn; mark.leach@xjtlu.edu.cn; enggee.lim@xjtlu.edu.cn; zhao.wang@xjtlu.edu.cn; jingchen.wang@xjtlu.edu.cn; zhenzhen.jiang@xjtlu.edu.cn).

Chaoyun Song is with the School of Engineering and Physical Sciences, Heriot-Watt University, EH14 4AS Edinburgh, U.K. (e-mail: c.song@hw.ac.uk).

Wenzhang Zhang and Yi Huang are with the Department of Electrical Engineering and Electronics, University of Liverpool, L69 3GJ Liverpool, U.K. (e-mail: pswzhan9@liverpool.ac.uk; huangyi@liverpool.ac.uk).

Color versions of one or more of the figures in this article are available online at http://ieeexplore.ieee.org.

Digital Object Identifier 10.1109/TII.2020.2983064

I. Introduction

With the increasing popularity of wearable electronic devices, wearable antenna designs have attracted much attention. Wearable antenna designs need to address multiple challenges including, the effects of the human body on performance, e.g., frequency shifting, efficiency degradation and radiation distortion when they are in close proximity; in addition, there are strict rules that limit the specific absorption rate (SAR) for body tissues. Wearable antennas should also be relatively flexible and ergonomic to accommodate daily human movement. One promising solution that could meet the above criterion is to exploit any existing metal structures on clothing or accessories as the antenna [1]–[8]. Examples of these include button antenna designs [1]–[4], watch strap antenna designs [5], zipper antenna designs [6], and belt antenna designs [7], [8]. These antenna designs would benefit from the conductivity and rigidness of the metal. However, they also suffer from limitations in regards to the shape and size of the wearable accessories.

An alternative direction is to base the antenna design on conducting textile material [9]–[22]. Most of these textile antennas are planar in shape and low profile. To reduce backward radiation and the effects of the human body on antenna performance, a full ground plane [9], [10], multilayer structure [11], and an electromagnetic band-gap (EBG) substrate layer [12]–[18] have been applied in previous studies. Moreover, a metallic button structure was used on conductive textile material to achieve reconfigurable antenna performance [19]. The effect of crumpling and bending of planar antennas has been studied in detail [20]–[22], which is significant where the antenna is intended for real-world wearable applications. Reliable fabrication procedures for multilayer conductive textile antenna have also been studied [23].

In this article, a novel belt antenna design is proposed for use in a smart belt system. A belt with a metal buckle is an ideal platform to integrate wearable electronics because of not only its metal part but also its popularity in daily life. The idea of a belt antenna has been considered in previous studies [7], [8], however, these studies did not consider the effect of the human body in detail. In this work, the effect of the body has been

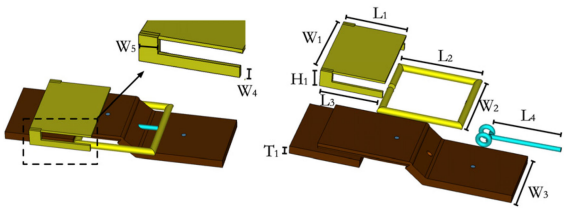

Fig. 1. Geometry and key parameters of the belt antenna.

investigated in detail. Characteristic mode analysis (CMA) has been applied to direct the structural design of the belt's metal fixtures to achieve a desirable current distribution. CMA offers two advantages in the design of such antennas; first, there are typically restrictions in belt buckle shape and size that can be used to provide an initial structure for the eigencurrent analysis. Second, since the field distribution and hence the radiation pattern is closely related to the current modes, by analyzing and selecting a specific current mode, the radiation pattern of the wearable antenna can be carefully designed to be steered away from the human body. This helps to reduce the SAR (SAR) in the body as well as the effect of the human body on antenna performance.

A conductive textile EBG ground plane is proposed to further reduce radiation toward the human body and enhance antenna gain and efficiency. A suspended transmission line model is used to evaluate the performance of several EBG designs under bending conditions.

The proposed structure could be applied in a smart belt system by way of a Bluetooth low energy (BLE) connection between the smart belt and electronic devices like a cellphone to provide many potential functions such as body condition monitoring, property loss prevention, localization or a falling-over alarm. A prototype of a smart belt system utilizing the antenna has been constructed to demonstrate its value.

The remainder of this article is divided into the following sections. Section II presents the geometry of the belt antenna and the textile EBG ground plane. Section III covers the CMA using Altair's FEKO simulation software. Section IV includes a comparison between two common EBG structures. The size, bandwidth, and effects of structural bending are analyzed and corresponding results are presented. Section V provides comparisons of simulated and measured results for the belt antenna system. Also, a prototype smart belt system is deployed, and simple functions were realized. Finally, Section VI concludes this article.

II. Antenna and Ground Geometry

The designed belt antenna is shown in Fig. 1. The metal parts include the belt buckle, the metal cap and two holding arms for the metal cap. The material selected for these parts is brass. For ease of manufacturing, the belt pin was 3-D printed from high strength ABS material. In the belt buckle, a small gap was left to fit an SubMiniature version A (SMA) connector as a feed. The relative dielectric constant of the leather was measured to be 2 using a Keysight N1501 probe. The loss tangent of the leather was measured to be 0.16. The final dimensions of the design are summarized in Table I.

TABLE I
Antenna Geometry Parameters

Symbol	Quantity	Value (mm)
W_1	width of the metal cap	31
W_2	width of the belt loop	31
W_3	width of the leather	25
W_4	width of the cap holding arm	3
W_5	width of the cap holding arm	5
L_1	length of the metal cap	27
L_2	length of the belt loop	30
L_3	length of the holding arm	16
L_4	length of the belt pin	25.5
H_1	height of the holding arm	7.6
T_1	thickness of the leather	3.6

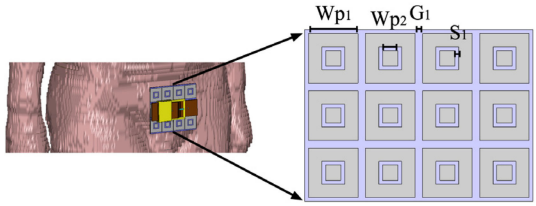

Fig. 2. Geometry and key parameters of the textile EBG ground.

TABLE II
EBG Geometry Parameters

Symbol	Quantity	Value (mm)
Wp_1	outer width of the square	26
Wp_2	inner width of the square	8
G_1	gap between two unit cells	4
S_1	width of inner square track	2

The textile EBG ground selected is shown in Fig. 2. The top concentric squares and the bottom ground plane are made of conductive fibers produced by the Yuanjinmei Glass Company in Foshan, China. The conducting fibers were attached to the textile substrate using a thin layer of conductive glue. The substrate layer was space cotton with a relative dielectric constant of 1.6. The final dimensions of the design are summarized in Table II.

III. Design Process of the Belt Antenna

A. Theory of Characteristic Modes

For conciseness, only some key concepts and mathematical formulations are included here. The characteristic modes analysis can be done using the eigenvalue equation $\boldsymbol{X}J_n = \lambda_n \boldsymbol{R}J_n$ [24], [25] where matrices $\boldsymbol{R}$ and $\boldsymbol{X}$ are the real and imaginary Hermitian parts of the impedance operator $\boldsymbol{Z} = \boldsymbol{R} + j\boldsymbol{X}$ [26]. The characteristic modes or characteristic currents $\boldsymbol{J}_n$ here can be

interpreted as the real currents flowing on the conducting body. Being independent of any source or excitation, the characteristic currents only depend on the shape and size of the conductor itself. The eigenvalue λ_n is always real, whose magnitude describes how well the nth characteristic mode radiates. When a mode resonates, the absolute value of λ_n is 0. The absolute value is used as the eigenvalue but can be either positive (storing magnetic energy) or negative (storing electric energy). As summarized in [26], the total current $\boldsymbol{J}$ can be expressed by the following equation:

$$\boldsymbol{J} = \sum \frac{V_n^i \boldsymbol{J}_n}{1 + j\lambda_n}. \tag{1}$$

The total current is seen to be inversely dependent on the eigenvalue λ_n. Thus, the term $|1/1 + j\lambda_n|$ is more commonly used to characterize the current distribution and evaluate how well a mode resonates. This term is called the model significance (MS), which has a range between 0 and 1 and is independent of any sources or excitations. When MS is 1, the model is resonant and will radiate most efficiently. V_n^i in (1) is the model-excitation coefficient and is defined as

$$V_n^i = \langle J_n, E^i \rangle = \oint_n J_n \bullet E^i ds. \tag{2}$$

This term quantifies how the excitation influences the contribution of each current mode to the total current. The term $\boldsymbol{V}_n^i \boldsymbol{J}_n$ denotes the coupling of the excitation (could be antenna feed or incident field) and the nth current mode; it determines whether a specific mode is properly excited by the excitation source. This term also provides a conceptual guideline for placing the excitation, which should induce an electrical field or current with strong coupling to the desired model current.

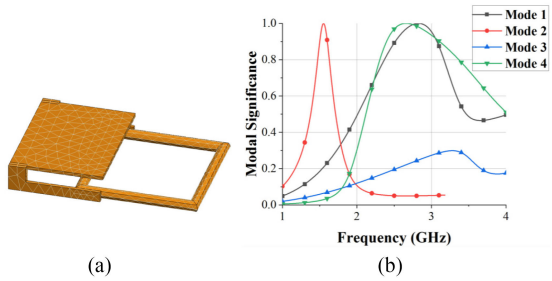

Fig. 3. CMA analysis of the belt. (a) Meshed metal structure of the belt buckle. (b) MS.

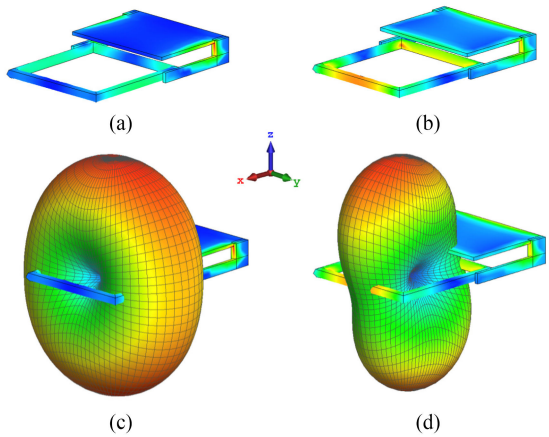

Fig. 4. Current distribution and corresponding radiation pattern for different characteristic modes. (a) Current distribution of mode 1. (b) Current distribution of mode 4. (c) Radiation pattern for mode 1. (d) Radiation pattern for mode 4.

B. CMA for the Belt Structure

CMA was used to test the feasibility of the initial design and provide a range for further parametric study. Intuitively, the basic shape of the belt buckle will lead to a current distribution and radiation pattern similar to that of a loop antenna. However, if the belt antenna follows the radiation pattern of a conventional one-wavelength loop, a considerably large portion (up to half) of the energy will be directed toward the human body leading to a relatively low radiation efficiency and limitations on output power due to SAR regulations. Also, antenna performance would be particularly sensitive to the condition of the human body behind it (clothing, fat to muscle ratio, etc.). Utilizing a metal cap, as shown in Fig. 1, commonly used to hold the end of the belt in place, radiation can be better directed away from the body.

The characteristic modes for the shape of the belt buck and holding cap were analyzed. To save computational complexity, only the metal parts are considered, the leather belt, which is essentially a lossy dielectric material, is not included at this stage. Initial CMA was performed to the proposed belt metal structure. The analysis at this stage did not include the excitation source or the feeding gap. The meshed radiating element and the corresponding MS are shown in Fig. 3. The MS illustrates that at 2.45 GHz there are two near-resonant modes: mode 1 and mode 4. The specific current distribution for these two modes and the radiation pattern are illustrated in Fig. 4. For the current distribution of mode 1, the current maximums are concentrated on the two sides of the buckle (along the x-axis), along the same two sides of the cap and in the corner of the connecting arms. The resulting radiation pattern is shown in Fig. 4(c). The pattern is almost omnidirectional in the yoz plane. In real-life scenarios, the human body will be located directly behind the metal buckle, in the negative z-direction. The omnidirectional property of mode 1 would mean that approximately half of the radiation would be directed toward the human body. This would cause a low radiation efficiency and a high SAR.

Meanwhile, for mode 4, the current maximums are concentrated on the belt buckle arms aligning with the y-axis. The main benefit of this mode is that there is a significant amount of current flow on the metal cap. The radiation pattern of this mode is bidirectional, as shown in Fig. 4(d). This offers the potential to increase the radiation in the positive z-direction, which is away from the human body. To achieve this the aim is to increase the current intensity on the cap and to make sure the current flow on the cap is in the same direction as the current flow on the buckle legs. By placing the feed and tuning the dimensions of the design, the intended current distribution on the metal cap can be achieved, resulting in more radiation directed

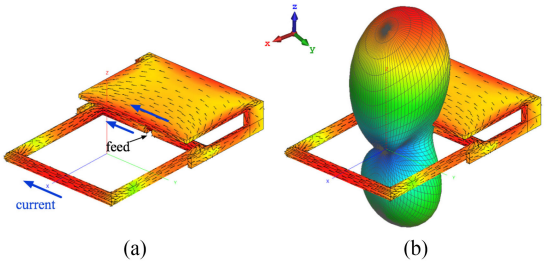

Fig. 5. Current distribution and corresponding radiation pattern for the characteristic mode 4 with size tuning and feed added. (a) Current distribution. (b) 3-D radiation pattern.

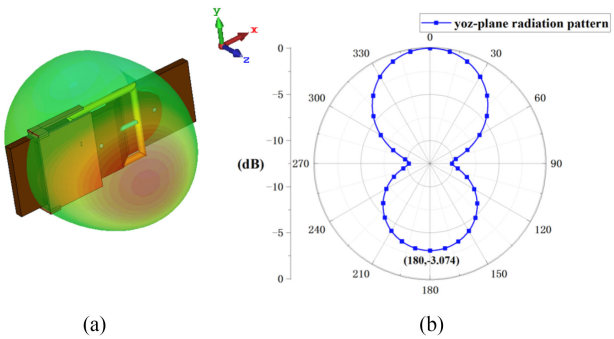

Fig. 6. Radiation pattern for the final belt design with all features added. (a) 3-D radiation pattern. (b) *yoz* plane cut.

away from the body. The optimal feed point was found to be at the buckle arm below the metal cap. In Fig. 5(a), the coupling between the excitation and the current flow, labeled with blue arrows, is maximized. With the excitation added, the radiation pattern, as shown in Fig. 5(b), exhibits an uneven distribution as more radiating energy is guided away from the body. With the metal radiating structure determined, other essential parts of the belt, the leather and the pin were added. Further optimization of the structure parameters was required after these dielectric materials were added. The full belt antenna model was simulated in free space using Computer Simulation Technology (CST) Microwave Studio; the 3-D radiation pattern is shown in Fig. 6(a). The *yoz* plane cut of the normalized radiation pattern is shown in Fig. 6(b). It can be seen that a 3-dB front-to-back ratio is obtained with this belt structure. Further simulations using the CST human voxel model were performed to check the response of the structure in its proposed operating environment, around the waist of the model.

C. Effect of the Human Body on the Antenna

When the belt antenna is placed close to the human body using the CST voxel human body model Gustav, a frequency shift is observed in comparison to the free space case. In the simulation, the belt leather is closely attached to the voxel model, leaving a distance of 3.6 mm (the thickness of the leather) between the radiating belt buckle and the human body model. As this situation reflects the principle usage of such an antenna, the parameters

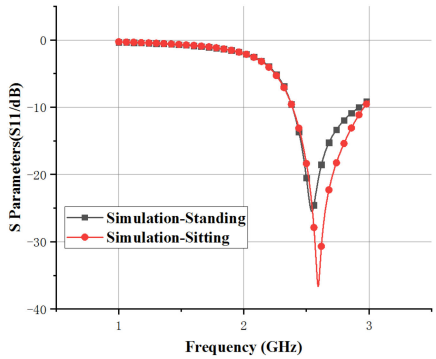

Fig. 7. Simulated *S* parameters of the belt antenna including voxel human model with two common postures.

TABLE III
RADIATION PERFORMANCE OF THE ANTENNA AT 2.45 GHZ

Postion	Radiation Efficiency (%)	Realized Gain (dBi)
Standing	54.36	4.373
Sitting	46.78	3.989

are further optimized to compensate for the frequency shift and the resulting antenna parameters are those in Table I.

The main beamwidth of the belt antenna has been considered in two common body positions, standing straight and sitting down. The reflection coefficient (S_{11}) of the antenna for each of these positions is shown in Fig. 7. In the sitting position, a greater level of absorption from the thigh causes a decrease in S_{11} and a slight frequency shift.

For wearable applications, the antenna radiation efficiency is a crucial indicator of antenna performance. Using the lossy voxel human body model, the resulting radiation efficiency for each body position at 2.45 GHz is given in Table III. Despite more radiation being guided away from the body due to the belt cap, (recall the 3-dB front-to-back ratio in the previous section), the radiation efficiency is still only around 50%. The radiation efficiency is slightly lower for the sitting scenario as there is more absorption from the thigh, which is consistent with the S_{11} results. The realized gain, including the mismatch loss as shown in Table III, confirms that the sitting position reduces the gain by almost 0.4 dB. The 3-D *in situ* radiation patterns for the two positions are shown in Fig. 8 with normalized 2-D E-plane and H-plane cuts shown in Fig. 9.

Due to the proximity of the antenna to the human body, SAR regulations must be considered. There are two common regulatory values for SAR on human body tissues, the first is imposed by the International Commission on Non-Ionizing Radiation Protection (ICNIRP) [27], which generally requires a maximum SAR value of 2 W/kg averaged over every 10 g of tissue. The second standard is from the Federal Communications Commission (FCC), which requires a maximum SAR of 1.6 W/kg averaged over each 1 g of tissue [28].

In Table IV, the SAR value was obtained by simulation according to the FCC standard and with the averaging method

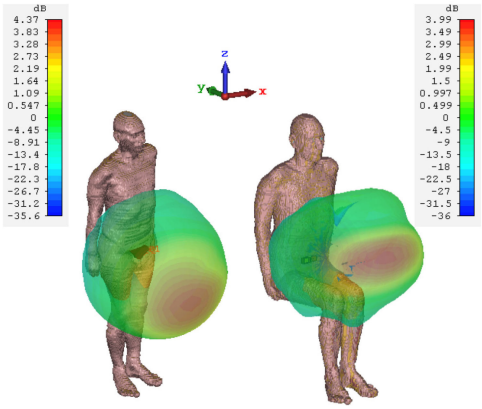

Fig. 8. Simulated realized gain (dBi) of the belt antenna including voxel human model with two common postures at 2.45 GHz.

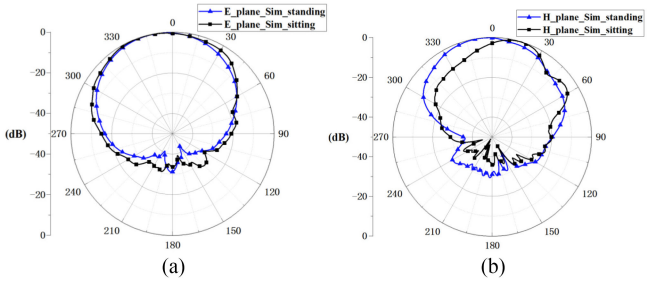

Fig. 9. Simulated E-plane and H-plane for including voxel human model with two common postures at 2.45 GHz. (a) E-plane. (b) H-plane.

TABLE IV
SAR VALUE OF THE BELT ANTENNA AT 2.45 GHZ

Postion	SAR (1g)	SAR (10g)
Standing	8.03 W/kg	2.71 W/kg
Sitting	3.16 W/kg	1.67 /kg

TABLE V
MAXIMUM INPUT POWER TO MEET SAR REGULATIONS

Postion	ICNIRP (2W/kg for 10g)	FCC (1.6W/kg for 1g)
Standing	370 mW	100 mW
Sitting	600 mW	190 mW

stated in IEEE/IEC 62704-1 [29], for an input power of 0.5 W. Simulated input power limitations for the antenna based on the ICNIRP and FCC standards are shown in Table V. This input power is far in excess of that used by the BLE system proposed in this study, which would have a maximum output power of 0 dBm (i.e., 1 mW) [30]. The SAR distribution averaged over 10 g is shown in Fig. 10. In both sitting and standing conditions, the maximal SAR was concentrated beneath the center of the belt buckle loop.

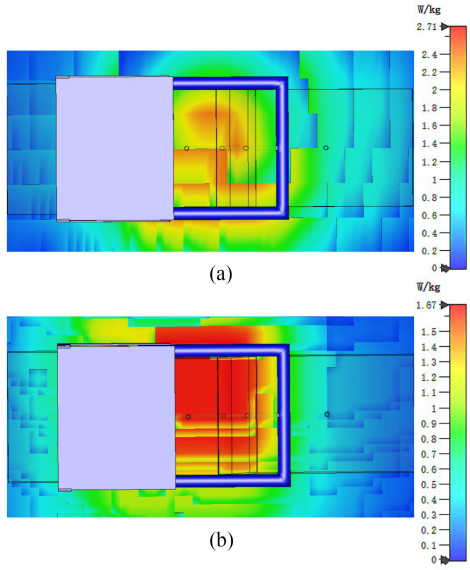

Fig. 10. SAR distribution of the belt antenna without the EBG. (a) Distribution with the standing model averaged over 10-g tissue. (b) Distribution with the sitting model averaged over 10-g tissue.

In this section, the antenna performance with the presence of the human body was studied. In order to determine the performance enhancement of this design quantitatively, the structure presented in [8] was used as a comparison. Since the radiation pattern and accurate efficiency data were not provided in the original paper, the design was modeled and simulated in our simulation environment. At its design frequency, 1.8 GHz, the radiation pattern is similar to a one-wavelength loop antenna, omnidirectional in the vertical plane, resulting in almost half of the radiated energy being directed toward the human body. The antenna has a radiation efficiency of 19.01 % when applied to the same voxel human body model used in the previous section. The proposed belt antenna in this study achieved 54.35 % under the same conditions. This numerical comparison demonstrates the effectiveness of the belt structure presented in this study.

IV. ANALYSIS OF TEXTILE EBG GROUND PLANE

From the previous section, the performance of the belt antenna can be considered appropriate for establishing a BLE link for a smart belt application. However, the efficiency of the antenna is still significantly influenced by the human body. Also, if the belt antenna was to be used in applications requiring a higher antenna input power level, for example, the latest Bluetooth 5 protocol that has a maximal output power of 20 dBm [31], SAR limitations could still present a problem. In real-life applications, a belt is commonly worn with pants or trousers located between the belt and the human body. The utilization of this material area offers the potential to further improve antenna performance. For example, by placing a ground plane between the antenna and the human body, the efficiency and gain of the on-body antenna can be increased. A conventional metallic ground would need to be located a distance of around a quarter of

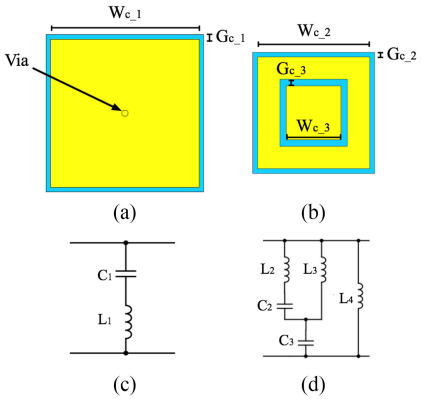

Fig. 11. Unit cell structure of two types of EBG structure and their equivalent circuits. (a) Square patches with vias. (b) Concentric squares. (c) Simplified equivalent circuit of square patches. (d) Simplified equivalent circuit for concentric squares.

the operating wavelength from the radiating element, otherwise, the mirrored currents due to the ground plane would interfere destructively with currents in the radiating element, reducing radiation efficiency. For the belt antenna scenario, leaving a quarter wavelength distance or using high dielectric constant materials to reduce the distance is not realistic.

Using an EBG structure as a ground plane woven into the garment worn between belt and body would allow the ground plane to be placed directly beneath the radiating element. It should be noted that the EBG structures in this study have been denoted as high impedance surfaces (HISs) or artificial magnetic conductors (AMCs) in other literature [12]–[15]. In previous studies, EBG substrates and ground plane layers have been applied to loop antennas and planar slot antennas to achieve low profile, high gain antenna performance [12]–[15]. In this study, the EBG structure is situated separately to the radiating element, thus acting more like a reflector located very close to the radiating element. Unlike the rigid belt structure, the textile EBG structure will experience a level of mechanical bending *in situ*. Also, effects like stretching make it difficult to model the textile EBG in simulation accurately. The process of textile EBG design is discussed in the following sections.

A. Comparison Between Two Common EBG Structures

Two of the most commonly applied EBG structures, square patches with vias (also named mushroom-like structures) and concentric squares, are analyzed according to this specific application scenario. The unit cell design of the two types of EBG is shown in Fig. 11(a) and (b). It should be noted that concentric squares can provide dual band-gap properties and are commonly applied with dual-band antenna though in this design only a single band was targeted.

The simplified equivalent circuits of the two structures are also shown in Fig. 11. The conducting loop of the square structure is characterized as inductance L_1 and the interelement capacitance is characterized as capacitance C_1. For the concentric square structure, the conducting central loop is characterized by inductance L_2. The outer loop is characterized by inductance

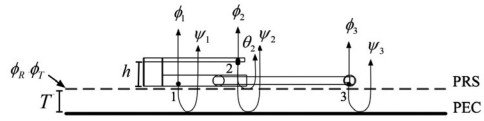

Fig. 12. Cavity model with ray analysis for the EBG ground plane and the belt antenna (PRS: partial reflective surface, PEC: perfect electric conductor).

L_3 and the ground plane is characterized by inductance L_4. The gap between the outer and inner loops gives rise to capacitance C_2 and the interelement capacitance is denoted by capacitance C_3. The resonant frequency of each structure can be determined from the capacitances and inductances of the equivalent circuits.

For an EBG plane to be used as a ground plane, a resonant cavity model previously developed for a planar antenna with EBG surface can be used [32]. The main difference between other planar EBG ground plane designs and this textile EBG ground plane with the belt antenna is that the radiating element here is not on a flat plane, which leads to different distances between the partial reflective surface (PRS) and the main radiating sections. This relationship is illustrated in Fig. 12, in which three radiating subelements are labeled for detailed analysis. The upper layer of the textile EBG is denoted as a PRS and the bottom layer is denoted as a perfect electric conductor (PEC). The PRS has two significant parameters, the reflection phase coefficient ϕ_R and the transmission phase coefficient ϕ_T. The phase shift introduced by the PEC surface is π. Ray optics analysis, which has been used for high gain planar antennas with PRS [32], has been applied to analyze this scenario.

For subelements located at a distance h from the PRS (example point 2 in Fig. 12), the phase difference between the radiating wavefront (ϕ_i) and the reflected wave through the EBG cavity (ψ_i) is

$$\phi_i - \psi_i = 2\phi_T - \frac{4\pi(h+T)}{\lambda} - \pi \tag{3}$$

where the term T denotes the height of the cavity, which is the thickness of the textile material in this case. Once the type of textile material is determined, this value is a fixed value for the design.

For a microradiating element placed very close to the EBG ground plane (example points 1 and 3), the previous formula can be simplified to

$$\phi_i - \psi_i = 2\phi_T - \frac{4\pi T}{\lambda} - \pi. \tag{4}$$

When the radiating element is located a distance above the EBG plane, an additional wave reflected from the PRS needs to be considered. The phase difference between these two waves can be calculated using the following equation:

$$\phi_i - \theta_i = \phi_R - \frac{4\pi h}{\lambda}. \tag{5}$$

The structural design of this antenna and the EBG structure should be optimized with respect to the following boundary conditions to avoid cancelation between the original outgoing

wave and the reflected wave by consideration of

$$-\frac{\pi}{2} \leq \phi_i - \psi_i \leq \frac{\pi}{2} \tag{6}$$

$$-\frac{\pi}{2} \leq \phi_i - \theta_i \leq \frac{\pi}{2}. \tag{7}$$

The wavefront created by the *i*th subvolume element can then be denoted by

$$E_i = a_{i,1}e^{j(2\pi f_0 t_i + \phi_i)} + a_{i,2}e^{j(2\pi f_0 t_i + \theta_i)} + a_{i,3}e^{j(2\pi f_0 t_i + \psi_i)} \tag{8}$$

where a_i is the attenuation factor for a certain reflected wave from the *i*th subvolume and f_0 is the resonant frequency. The term ϕ_i denotes the directly radiated wave. The terms θ_i and ψ_i are the reflected wave from the PRS and the PEC, respectively. A graphical representation of these terms is given in Fig. 12.

The total wavefront can be expressed as a superposition of all the subvolume element waves by

$$E = g_k(E_1, E_2, E_3 \ldots, E_k) \tag{9}$$

where g_k represents the superposition.

This theoretical analysis provides a guideline for the optimization of the EBG design parameters. The phase of the reflected waves at each plane, one closely attached to the PRS and one elevated by a distance *h*, should be considered in the simulation. The reflected phase can be obtained in CST by adding a thin layer of air between the PRS and the Floquet port in the unit cell simulation. The ideal reflected phase is 0° from both planes. However, for a certain EBG design with fixed parameters, the reflected phase would change with the distances between the Floquet port, the PEC and the PRS. Thus, a middle ground where the reflected phases at the two planes were both very close to zero was selected. Detailed dimensions of the concentric square EBG unit cell are listed in Table II. For the square patches with vias, each edge is 50 mm long and the gap between patches is 6 mm.

Comparing the two types of EBG design, the square patches with vias design is almost four times larger in size than the concentric square design. Moreover, the via structure used to suppress the surface wave is much more difficult to fabricate with textile materials.

B. Effect of Bending

Fig. 11 shows that the capacitance formed by the gap between unit cells or within each unit cell is crucial in determining the resonant frequency of the EBG structure. When the textile EBG is applied on the human body, the bending of the material may cause changes in capacitance and influence the resonant frequency, therefore this influence must be evaluated. The reflected phase can be obtained through simulation using the CST unit cell boundary condition, however, it is difficult to either perform the reflection phase simulation over the entire textile ground or perform actual measurements of the reflected phase, especially in bending conditions. Therefore, the suspended transmission line method has been used to evaluate the performance of the entire EBG structure under bending conditions. The suspended transmission line method places a separated transmission line elevated a given distance above the EBG ground. The transmission coefficient (S_{21}) along the line is then used to characterize the band-gap of the EBG structure. The S_{21} value can be directly obtained using a network analyzer; the experimental set-up is shown in Fig. 18(c). This method has been used in previous studies to determine the resonating frequency for EBG/AMC structures [13]. To the best of the authors' knowledge, this is the first time that such a method has been applied in the evaluation of bending effects for textile EBG material.

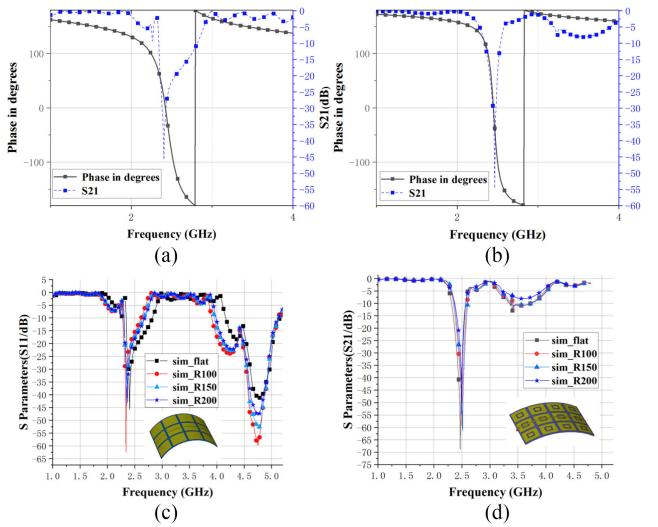

Fig. 13. Comparison between the reflected phase of the EBG structure and the S_{21} of the corresponding suspended transmission line. (a) Reflected phase and band-gap for square patches with vias EBG structure. (b) Reflected phase and band-gap for concentric squares EBG structure. (c) Band-gap of the square patches with vias EBG structure when bent. (d) Band-gap of the concentric squares EBG structure when bent.

Fig. 13(a) and (b) shows the simulation results characterizing the relationship between the reflected phase and EBG band-gap for each EBG type, square and concentric square, respectively. The band-gap of each design was determined from the S_{21} of the suspended transmission line experiment. The ideal reflected phase of 0° was located approximately at the center of the band-gap. From both the reflected phase and the band-gap, it can be seen that the square patches with vias structure would provide a wider bandwidth compared to the concentric squares structure. This is the main benefit of the square patches structure.

Fig. 13(c) and (d) shows the effect of bending on the band-gap of the two EBG structures evaluated using suspended transmission line simulation. The structures were bent toward a cylinder with radii of 100, 150, and 200 mm.

From the figures, it can be seen that for both structures the bending leads to a slight reduction in bandwidth. The square patches structure has a larger bandwidth, however, for the targeted BLE application, the concentric squares structure provides sufficient bandwidth and is preferable due to its smaller size and fabrication simplicity.

Fig. 14 supports the use of the suspended transmission line method in determining the properties of the EBG ground plane.

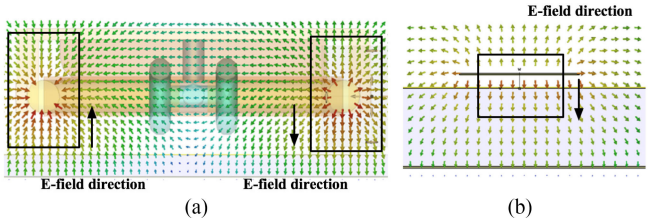

Fig. 14. Comparison between fields. (a) E-field of the belt antenna over the EBG plane. (b) E-field of the suspended transmission line.

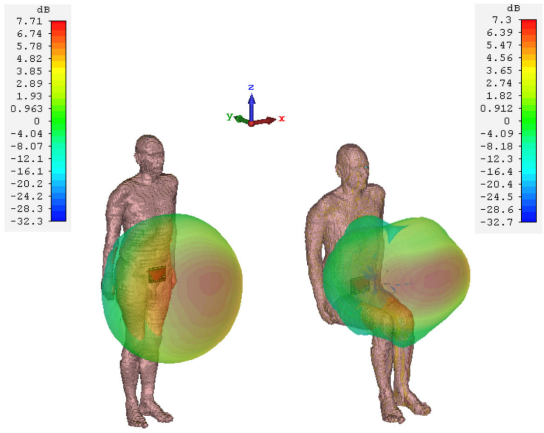

Fig. 15. Simulated radiation pattern and realized gain of the belt antenna with EBG ground plane.

The E-field cross-sectional plots show that the main radiating fields toward the EBG in the case of both the belt antenna and the suspended transmission line are perpendicular to the EBG. Thus, the band-gaps seen by the radiated field in these two cases are similar.

C. Antenna Performance With Textile Ground Plane

The belt antenna with the textile EBG ground plane has been simulated using the voxel model in CST with two different postures. The 3-D far-field results are shown in Fig. 15.

The radiation pattern is very similar to that observed without the textile EBG. However, the maximum realized gain significantly increases with the help of the textile EBG.

Aside from the radiation pattern, the radiation efficiency and SAR value are two very important figures for wearable antenna applications. The application of the textile EBG plane has improved the belt antenna performance in these two aspects, as shown in Table VII. An increase in radiation efficiency and a reduction in SAR value can be achieved due to the isolation and reflection of the textile EBG ground plane. The SAR value distribution is shown in Fig. 16. It should be noted that, due to the isolation of the textile EBG, the maximal SAR in the sitting condition was located at the right thigh close to the belt metal cap.

D. Effect of Different Human Body

The simulation process in the previous sections used only the Gustav model in the CST voxel family, which is a model

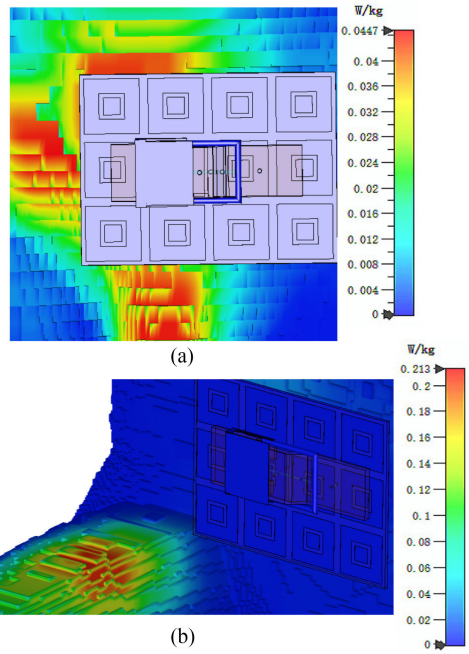

Fig. 16. SAR distribution of the belt antenna with the EBG. (a) Distribution with the standing model averaged over 10-g tissue. (b) Distribution with the sitting model averaged over 10-g tissue.

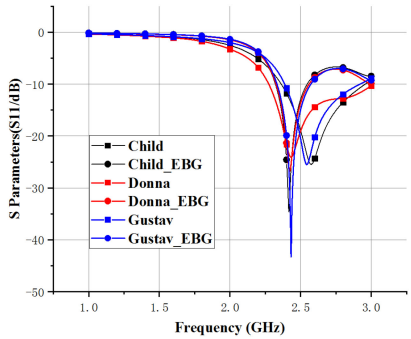

Fig. 17. *S* parameters of the antenna with/without textile EBG on different voxel human models.

of a 38-year-old male (176 cm, 69 kg). With different body shapes, the tissue composition would vary and thus result in different electrical properties. To evaluate the effect of different body shapes on the antenna performance, two other body models from the CST voxel family, Donna (40-year-old female, 176 cm, 79 kg) and Child (7-year-old female, 115 cm, 21.7 kg), were also applied in the simulation. The reflection coefficients for different body models are shown in Fig. 17 and the radiation parameters are summarized in Table VI. Without the textile EBG, frequency shifts and changes in radiation efficiency and gain can be observed with different human body models. When the textile EBG is used, the effect of the human body was significantly reduced. The belt antenna backed with the textile EBG offers stable performance when applied to people with different body shapes.

TABLE VI
COMPARISON OF ANTENNA PERFORMANCE WITH DIFFERENT HUMAN BODY MODEL

Model	Radiation Efficiency (%)	Realized Gain (dBi)
Gustav	54.36	4.37
Gustav_EBG	84.11	7.70
Donna	49.56	1.87
Donna_EBG	83.96	7.57
Child	47.78	2.06
Child_EBG	84.24	7.59

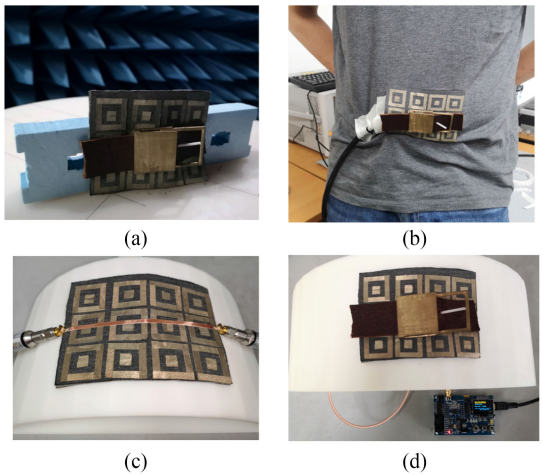

Fig. 18. Fabricated prototype and measurement set-up. (a) Radiation pattern measurement in the anechoic chamber. (b) Testing on the real human body. (c) Suspended transmission line test for textile EBG. (d) Prototype integrated with the BLE module.

V. RESULTS AND THE PROPOSED SYSTEM

A. Fabricated Belt Antenna and Textile EBG Ground Plane

The metal part of the belt antenna was fabricated by 3-D printing brass, whereas the belt pin was 3-D printed from high-intensity ABS material. Three cylinder parts were also made by 3-D printing to measure the band-gap of the textile EBG under bending conditions. The fabricated antenna and EBG, along with the testing conditions, are shown in Fig. 18. Before being applied to the belt antenna, the textile EBG was first evaluated with a suspended transmission line and the results are shown in Fig. 19.

The measured results indicate a slight frequency shift and a larger bandwidth in comparison to the simulation result. This is mainly due to the inability to accurately model the electrical properties of the conducting fiber, especially under the effects of bending and stretching. Also, the measured results show that the band-gap of the fabricated EBG covers the desired band and can be applied with the belt antenna.

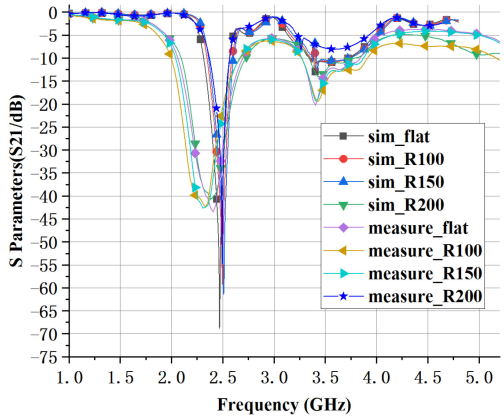

Fig. 19. Simulated and measured band-gap for the suspended transmission line over concentric square textile EBG ground plane.

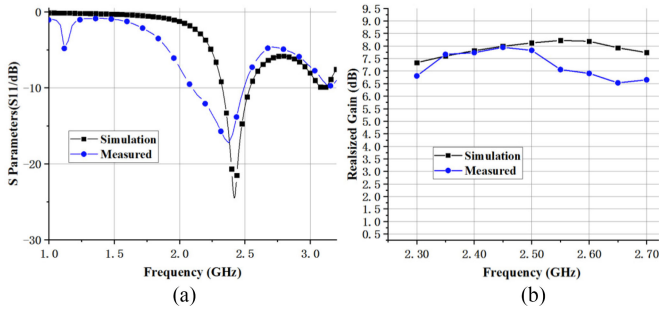

Fig. 20. Simulated and measured results. (a) S_{11} for the belt antenna with the textile EBG ground plane. (b) Realized gain over frequency.

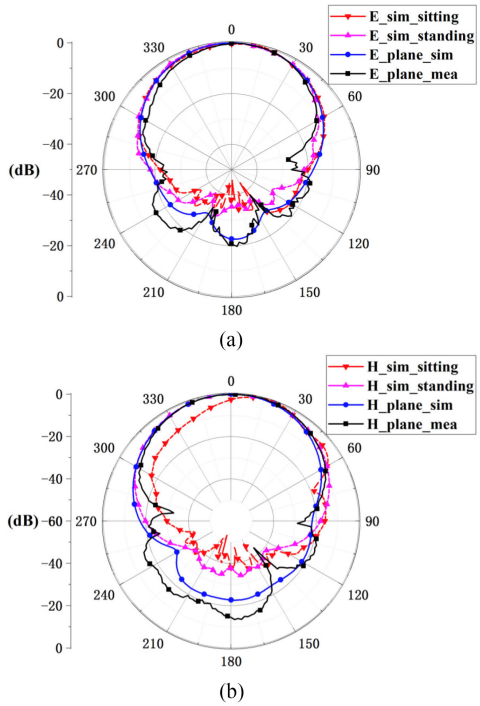

Fig. 21. Comparison between simulated and measured radiation pattern for the belt antenna with textile EBG ground plane (simulation with standing and sitting voxel model also included). (a) E-plane. (b) H-plane.

TABLE VII
COMPARISON OF ANTENNA PERFORMANCE WITH/WITHOUT TEXTILE GROUND AND WITH OTHER SYSTEMS

Ref.	Antenna Type	Radiation Efficiency (%)	Realized Gain (dBi) (sim/mea)	SAR (10g, with 0.5 W input) (W/kg)
This Work	Standing with EBG	84.11	7.70/7.15	0.04
	Standing without EBG	54.36	4.37/4.01	2.71
	Sitting with EBG	67.77	7.30/-	0.21
	Sitting without EBG	46.78	3.98/-	1.67
	Free space with EBG	86.25	7.98/7.94*	N/A
[8]	Replicated belt antenna design	19.01	-1.33/-	N/A
[14]	Textile antenna with EBG structure	61.30	5.20/-	0.37
[33]	Button with textile ground	72.10	5.16/1.1*	0.176 (32 mW input)
[34]	Smart watch frame antenna	26.00	-0.89/3.8*	N/A
[35]	Loop over high impedance surface	40.00	4.20/3.00	0.55 (100 mW input)

*The gain measured is free space gain, without actual human or phantom presence.

The measured S_{11} and radiation patterns are shown in Figs. 20(a) and 21(a) and (b), respectively. The measured maximal realized gain versus frequency is shown in Fig. 20(b). The measurements were performed in our in-house anechoic chamber. A low permittivity foam was used as the support structure on the rotary table. Generally, the measured results match the simulations well. Some discrepancies occurred in the radiation pattern measurement at 90° and 270° in both the E-plane and H-plane. This was due to the slight curvature of the lossy belt leather and the textile EBG when they are closely attached. The measured radiation pattern matches the simulated radiation pattern with the sitting/standing voxel human model well in the direction of the main lobe. However, a larger back lobe can be observed due to the lack of the body tissue absorption.

Both free space and on-body realized gain were measured. The antenna was attached to the waist of a human subject (188 cm, 81 kg) in the chamber to measure the on-body realized gain. The measured maximal realized gain of the belt antenna with textile EBG at 2.45 GHz was 7.94 dBi without human presence and 7.15 dBi when the antenna was attached to the human waist.

A comparison between the proposed belt antenna and some related state-of-the-art wearable antenna solutions is included in Table VII. The results with/without the textile EBG on different voxel model structures (standing model and sitting model) are all included. It should be noted that in this study, CST voxel models were used to evaluate the human body effect on the antenna performance and the value of SAR was calculated according to IEEE/IEC 62704-1 with a 0.5 W input power [29]. The simulation condition for [8] and [14] in Table VII was identical to the condition used in this study. In [33], a partial uniform human body model was employed, whereas the SAR was evaluated with the same standard but with an input power of 32 mW. In [34], a one-layer wrist model was used for evaluation. In [35], a four-layer human tissue model was used. The SAR was evaluated with the same standard, whereas the input power was set to be 100 mW. Moreover, a noticeable difference in the simulated and measured realized gain values can be seen for [33] and [34] in Table VII. This is due to that the provided simulated value was with the human body models, whereas the measurements were performed in free space scenario. For the design in [33], the human body would have a significant reflecting effect and hence the on-body gain would be higher. Meanwhile in [34], the effect of body tissue absorption was more significant than reflection. Therefore the on-body realized gain was lower. For the proposed belt antenna with EBG, the measured free space and on-body realized gain was quite consistent thanks to the textile EBG structure.

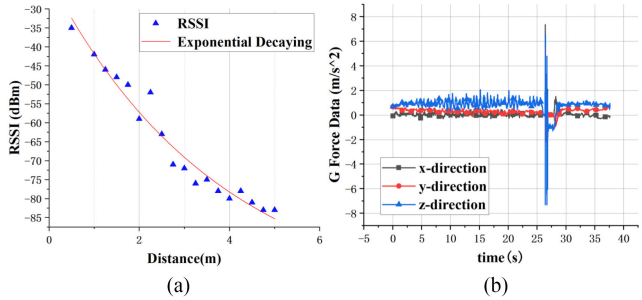

(a) (b)

Fig. 22. Smart belt prototype. (a) BLE RSSI on the cellphone at different distances. (b) Data from the gyroscope onboard the smart belt system.

The measurements were performed in our in-house anechoic chamber (length: 6 m, width: 4 m, height: 3 m) and the antenna was attached to a human subject (188 cm, 81 kg) for on-body measurements. Generally, all evaluations of the prior-art results in Table VII and our work were performed under a similar experimental condition and therefore the results are comparable and promising. Overall, the proposed belt antenna achieved a higher realized gain and a lower SAR value due to the structural design and the isolation/reflection provided by the textile EBG.

B. Smart Belt Prototype With Simple Functions

A smart belt prototype system was developed using a Texas Instrument CC2401 BLE chip and a developer board obtained from the company AmoMcu. A link between the smart belt and an Android cellphone was set up and the output power for the chip was set to be –10 dBm. The relationship between the received signal strength indicator (RSSI) and line-of-sight distance in the lab is shown in Fig. 22(a). The raw data were not enough to provide accurate distance measurement and was largely influenced by the surrounding environment. The data can still be used to make sure the cell phone stays in Bluetooth

range of the belt and the range can be changed by setting the input power.

An onboard gyroscope was integrated into the smart belt prototype. In Fig. 22(b), data from 40 s of walking and a simulated falling over were recorded. The simulated falling over happened at the 26th second on the timeline and a sharp increase in the acceleration in the z-direction can be observed at that moment. The smart belt system can provide a falling over alarm for the elderly.

The belt antenna with the textile EBG ground plane has a high efficiency when placed in close proximity with the human body and a low SAR value toward the body. When applied in the smart belt system, it can reduce requirements on the power and battery.

VI. Conclusion

In this article, a belt antenna was designed with the aid of CMA. The effect of the human body was closely evaluated throughout the design process. It was found that CMA was of great use in determining the design parameters and placing the feed. This belt antenna design was able to direct more radiated energy away from the human body. Thus, the radiation efficiency was increased, whereas the SAR value was reduced.

The belt antenna on its own can satisfy the BLE transmission requirement for the smart belt system. However, considering that the belt antenna could be operating over long periods of time and that the available battery size for the system would be quite limited, further improvements should be made regarding SAR and radiation efficiency. A separate textile EBG ground plane was developed to be integrated into the trousers behind the belt antenna. A set of optimization guidelines for designing the EBG with nonplanar wearable antennas were proposed. Also, the suspended transmission line method was proposed in this case to accurately determine the band-gap of the textile EBG, especially under bending conditions. The belt antenna together with the textile EBG formed a highly efficient and safe transmission mechanism for a smart belt system.

Acknowledgment

The authors would like to thank CST AG for providing the CST Studio Suite Electromagnetic Simulation Software package under the China Key University Promotion Program and the Municipal Key Lab for Wireless Broadband Access Technologies in the Department of Electrical Engineering, Xi'an Jiaotong Liverpool University.

References

[1] X. Y. Zhang, H. Wong, T. Mo, and Y. F. Cao, "Dual-band dual-mode button antenna for on-body and off-body communications," *IEEE Trans. Biomed. Circuits Syst.*, vol. 11, no. 4, pp. 933–941, Aug. 2017.

[2] H. Xiaomu, S. Yan, and G. A. E. Vandenbosch, "Wearable button antenna for dual-band WLAN applications with combined on and off-body radiation patterns," *IEEE Trans. Antennas Propag.*, vol. 65, no. 3, pp. 1384–1387, Mar. 2017.

[3] B. Sanz-Izquierdo, J. C. Batchelor, and M. I. Sobhy, "Button antenna on textiles for wireless local area network on body applications," *IET Microw., Antennas Propag.*, vol. 4, no. 11, pp. 1980–1987, Nov. 2010.

[4] S. J. Chen, T. Kaufmann, D. C. Ranasinghe, and C. Fumeaux, "A modular textile antenna design using snap-on buttons for wearable applications," *IEEE Trans. Antennas Propag.*, vol. 64, no. 3, pp. 894–903, Mar. 2016.

[5] G. Li, G. Gao, J. Bao, B. Yi, C. Song, and L. Bian, "A watch strap antenna for the applications of wearable systems," *IEEE Access*, vol. 5, pp. 10332–10338, 2017.

[6] G. Li, Y. Huang, G. Gao, X. Wei, Z. Tian, and L. Bian, "A handbag zipper antenna for the applications of body-centric wireless communications and Internet of Things," *IEEE Trans. Antennas Propag.*, vol. 65, no. 10, pp. 5137–5146, Oct. 2017.

[7] B. Sanz-Izquierdo and J. C. Batchelor, "A dual band belt antenna," in *Proc. Int. Workshop Antenna Technol., Small Antennas Novel Metamater.*, Chiba, Japan, 2008, pp. 374–377.

[8] D. Gaspar and A. A. Moreira, "Belt antenna for wearable applications," in *Proc. IEEE Antennas Propag. Soc. Int. Symp.*, Charleston, SC, USA, 2009, pp. 1–4.

[9] P. B. Samal, P. J. Soh, and G. A. E. Vandenbosch, "UWB all-textile antenna with full ground plane for off-body WBAN communications," *IEEE Trans. Antennas Propag.*, vol. 62, no. 1, pp. 102–108, Jan. 2014.

[10] G. Gao, C. Yang, B. Hu, R. Zhang, and S. Wang, "A wide-bandwidth wearable all-textile PIFA with dual resonance modes for 5 GHz WLAN applications," *IEEE Trans. Antennas Propag.*, vol. 67, no. 6, pp. 4206–4211, Jun. 2019.

[11] L. A. Y. Poffelie, P. J. Soh, S. Yan, and G. A. E. Vandenbosch, "A high-fidelity all-textile UWB antenna with low back radiation for off-body WBAN applications," *IEEE Trans. Antennas Propag.*, vol. 64, no. 2, pp. 757–760, Feb. 2016.

[12] S. Yan, P. J. Soh, and G. A. E. Vandenbosch, "Low-profile dual-band textile antenna with artificial magnetic conductor plane," *IEEE Trans. Antennas Propag.*, vol. 62, no. 12, pp. 6487–6490, Dec. 2014.

[13] S. Zhu and R. Langley, "Dual-band wearable textile antenna on an EBG substrate," *IEEE Trans. Antennas Propag.*, vol. 57, no. 4, pp. 926–935, Apr. 2009.

[14] M. Wang *et al.*, "Investigation of SAR reduction using flexible antenna with metamaterial structure in wireless body area network," *IEEE Trans. Antennas Propag.*, vol. 66, no. 6, pp. 3076–3086, Jun. 2018.

[15] A. Alemaryeen and S. Noghanian, "On-body low-profile textile antenna with artificial magnetic conductor," *IEEE Trans. Antennas Propag.*, vol. 67, no. 6, pp. 3649–3656, Jun. 2019.

[16] S. Kim, Y. Ren, H. Lee, A. Rida, S. Nikolaou, and M. M. Tentzeris, "Monopole antenna with inkjet-printed EBG array on paper substrate for wearable applications," *IEEE Antennas Wireless Propag. Lett.*, vol. 11, pp. 663–666, 2012.

[17] M. A. B. Abbasi, S. S. Nikolaou, M. A. Antoniades, M. N. Stevanović, and P. Vryonides, "Compact EBG-backed planar monopole for BAN wearable applications," *IEEE Trans. Antennas Propag.*, vol. 65, no. 2, pp. 453–463, Feb. 2017.

[18] G. Gao, C. Yang, B. Hu, R. Zhang, and S. Wang, "A wearable PIFA with an all-textile metasurface for 5 GHz WBAN applications," *IEEE Antennas Wireless Propag. Lett.*, vol. 18, pp. 288–292, 2019.

[19] S. J. Chen, D. C. Ranasinghe, and C. Fumeaux, "A robust snap-on button solution for reconfigurable wearable textile antennas," *IEEE Trans. Antennas Propag.*, vol. 66, no. 9, pp. 4541–4551, Sep. 2018.

[20] Q. Bai and R. Langley, "Crumpled integrated AMC antenna," *Electron. Lett.*, vol. 45, no. 13, pp. 662–663, Jun. 2009.

[21] Q. Bai and R. Langley, "Crumpling of PIFA textile antenna," *IEEE Trans. Antennas Propag.*, vol. 60, no. 1, pp. 63–70, Jan. 2012.

[22] L. Song and Y. Rahmat-Samii, "A systematic investigation of rectangular patch antenna bending effects for wearable applications," *IEEE Trans. Antennas Propag.*, vol. 66, no. 5, pp. 2219–2228, May 2018.

[23] R. Del-Rio-Ruiz, J. Lopez-Garde, J. Legarda, S. Lemey, O. Caytan, and H. Rogier, "Reliable lab-scale construction process for electromagnetically coupled textile microstrip patch antennas for the 2.45 GHz ISM band," *IEEE Antennas Wireless Propag. Lett.*, vol. 19, pp. 153–157, 2020.

[24] R. Garbacz and R. Turpin, "A generalized expansion for radiated and scattered fields," *IEEE Trans. Antennas Propag.*, vol. AP-19, no. 3, pp. 348–358, May 1971.

[25] R. Harrington and J. Mautz, "Theory of characteristic modes for conducting bodies," *IEEE Trans. Antennas Propag.*, vol. AP-19, no. 5, pp. 622–628, Sep. 1971.

[26] M. Cabedo-Fabres, E. Antonino-Daviu, A. Valero-Nogueira, and M. F. Bataller, "The theory of characteristic modes revisited: A contribution to the design of antennas for modern applications," *IEEE Antennas Propag. Mag.*, vol. 49, no. 5, pp. 52–68, Oct. 2007.

[27] International Commission on Non-Ionizing Radiation Protection, "Guidelines for limiting exposure to time-varying electric, magnetic, and electromagnetic fields (up to 300 GHz)," *Health Phys.*, vol. 74, pp. 494–522, Apr. 1998.
[28] Federal Communications Commission, "Specific absorption rate (SAR) for cellular telephones," 2016. [Online]. Available: https://www.fcc.gov/general/specific-absorption-rate-sar-cellular-telephones
[29] K. Chan, R. F. Cleveland, and D. L. Means, "Evaluating compliance with FCC guidelines for human exposure to radiofrequency electromagnetic fields," OET Bulletin 65, Dec. 1997.
[30] C. Gomez, J. Oller, and J. Paradells, "Overview and evaluation of Bluetooth low energy: An emerging low-power wireless technology," *Sensors*, vol. 12, pp. 11734–11753, 2012.
[31] M. Collotta, G. Pau, T. Talty, and O. K. Tonguz, "Bluetooth 5: A concrete step forward toward the IoT," *IEEE Commun. Mag.*, vol. 56, no. 7, pp. 125–131, Jul. 2018.
[32] A. P. Feresidis, G. Goussetis, W. Shenhong, and J. C. Vardaxoglou, "Artificial magnetic conductor surfaces and their application to low-profile high-gain planar antennas," *IEEE Trans. Antennas Propag.*, vol. 53, no. 1, pp. 209–215, Jan. 2005.
[33] S. Yan and G. A. E. Vandenbosch, "Design of wideband button antenna based on characteristic mode theory," *IEEE Trans. Biomed. Circuits Syst.*, vol. 12, no. 6, pp. 1383–1391, Dec. 2018.
[34] S. Su and Y. Hsieh, "Integrated metal-frame antenna for smartwatch wearable device," *IEEE Trans. Antennas Propag.*, vol. 63, no. 7, pp. 3301–3305, Jul. 2015.
[35] D. Wen, Y. Hao, M. O. Munoz, H. Wang, and H. Zhou, "A compact and low-profile MIMO antenna using a miniature circular high-impedance surface for wearable applications," *IEEE Trans. Antennas Propag.*, vol. 66, no. 1, pp. 96–104, Jan. 2018.

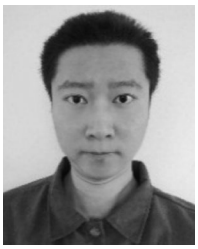

Rui Pei received the B.Eng. (Hons.) degree in telecommunication engineering from Xi'an Jiaotong Liverpool University, Suzhou, China and the University of Liverpool, Liverpool, U.K., in 2015, and the M.Sc. degree (with distinction) in signal processing and communications from the University of Edinburgh, Edinburgh, U.K., in 2016. He is currently working toward the Ph.D. degree in wireless communications and radio frequency engineering with the University of Liverpool.

His research interests include antenna design, wearable antennas, metamaterials, specific absorption rate, and body area networks.

Mark Paul Leach received the B.Eng. (Hons.) degree in communication and electronic engineering and the Ph.D. degree in electrical and electronic engineering from the University of Northumbria, Newcastle upon Tyne, U.K., in 1999 and 2005, respectively.

From 2003 to 2008, he was a Research Associate in the field of microwave holography. From 2008 to 2013, he was a Lecturer with the Seoul National University of Science and Technology, Seoul, South Korea, conducting research into thin films for photovoltaic applications. In 2013, he joined the Department of Electrical and Electronic Engineering, Xi'an Jiaotong Liverpool University, Suzhou, China, where he is currently the Head of Department. His research interests include antennas, radio frequency/microwave engineering, electromagnetic measurements/simulations, energy harvesting, wireless power/energy transfer, and wireless communication networks.

Eng Gee Lim (Senior Member, IEEE) received the B.Eng. (Hons.) and Ph.D. degrees in electrical and electronic engineering from the University of Northumbria, Newcastle upon Tyne, U.K., in 1998 and 2002, respectively.

From 2002 to 2007, he was with the Andrew Industries Ltd., Altham, U.K., a leading communications systems company. Since August 2007, he has been with Xi'an Jiaotong Liverpool University, Suzhou, China, where he was formally the Head of the Electrical and Electronic Engineering Department and University Dean of Research and Graduate studies. He is currently the School Dean of Advanced Technology, Director of Artificial Intelligence University Research Centre, and also Professor with the Department of Electrical and Electronic Engineering. He has authored/coauthored more than 100 refereed international journals and conference papers. His research interests include artificial intelligence, robotics, artificial intelligence + health care, international standard (ISO/IEC) in robotics, antennas, radio frequency/microwave engineering, electromagnetic measurements/simulations, energy harvesting, power/energy transfer, smart-grid communication; wireless communication networks for smart and green cities.

Prof. Lim is a Chartered Engineer and Fellow of both IET and Engineers Australia. He is also a Senior Fellow of HEA.

Zhao Wang received the B.Eng. degree in electronic and information engineering from Xi'an Jiaotong University, Xi'an, China, in 2003 and the Ph.D. degree in wireless communication and electromagnetics from the Queen Mary University of London, London, U.K., in 2009.

Since 2010, she has been with the Department of Electrical and Electronics Engineering, Xi'an Jiaotong Liverpool University, Suzhou, China, where she is currently an Associate Professor. Her research interests include antennas and the optimization algorithms, radio frequency and microwave engineering, energy harvesting, and wireless power transfer.

Chaoyun Song (Member, IEEE) received B.Eng., M.Sc., and Ph.D. degrees in electrical engineering and electronics from the University of Liverpool (UoL), Liverpool, U.K., in 2012, 2013, and 2017, respectively.

Between 2017 and 2020, he was a Postdoctoral Research Associate with the UoL. He is currently an Assistant Professor with the School of Engineering and Physical Sciences, Heriot-Watt University, Edinburgh, U.K. He has authored/coauthored more than 60 papers (including 30 IEEE transactions) in peer-reviewed journals and conference proceedings. He has held two U.S. patents and two U.K. patents. His research interests include wireless energy harvesting and wireless power transfer technologies, antennas and microwave circuits using novel materials, dielectric material and ionic liquids in radio frequency (RF) applications, metamaterials and metasurfaces in RF, energy harvesting, and sensing technologies.

Dr. Song was the recipient of many international awards such as the BAE Systems Chairman's Award in 2017 for the innovation of next-generation global navigation satellite system antennas. In 2018, he was the recipient of the highly commended award from the prestigious IET Innovation Awards over three categories: "Energy and Power," "Emerging Technologies," and "Young Innovators." He has been a regular Reviewer of more than 25 international journals including *Nature Communications*, *Applied Physics Letters*, *Nano Energy*, and seven IEEE transactions, and a Guest Editor for *Wireless Communications and Mobile Computing*.

Jingchen Wang received the M.Eng. degree in electrical and information engineering from Xi'an Jiaotong University, Xi'an, China, in 2013 and the Ph.D. degree in electrical engineering and electronics from the University of Liverpool, Liverpool, U.K., in 2019.

She is currently a Lecturer with the Department of Electrical and Electronic Engineering, Xi'an Jiaotong Liverpool University, Suzhou, China. Her research interests include wearable antennas, implantable antennas, wireless power transfer, energy harvesting, and 5G/5G+ wireless communications.

Dr. Wang has been a Reviewer for the IEEE TRANSACTIONS ON ANTENNAS AND PROPAGATION, IEEE ACCESS, IEEE TRANSACTIONS ON CIRCUITS AND SYSTEMS I: REGULAR PAPERS, and IEEE SENSORS JOURNAL.

Wenzhang Zhang received the M.Sc. (Hons.) degree in electrical engineering and electronics, in 2016, from the University of Liverpool, Liverpool, U.K., where she is currently working toward the Ph.D. degree in wireless communications and radio frequency engineering.

Her research interests include metasurface-based antenna, characteristic mode analysis, wearable antenna, and rectifying circuit.

Zhenzhen Jiang received the B.Eng. (Hons.) degree in telecommunication engineering in 2016 from Xi'an Jiaotong Liverpool University, Suzhou, China and the University of Liverpool, Liverpool, U.K., where she is currently working toward the Ph.D. degree in wireless communications and radio frequency engineering.

Her research interests include implantable antenna design, simultaneously wireless power and data transfer, energy harvesting, and wireless personal area networks applications.

Yi Huang (Senior Member, IEEE) received the B.Sc. degree in physics from Wuhan University, Wuhan, China, in 1984, the M.Sc. (Eng.) degree in microwave engineering from the Nanjing Research Institute of Electronics Technology (NRIET), Nanjing, China, in 1987, and the D.Phil. degree in communications from the University of Oxford, Oxford, U.K., in 1994.

His experience includes three years spent with NRIET as a Radar Engineer and various periods with the University of Birmingham, Birmingham, U.K.; University of Oxford; and University of Essex, Colchester, U.K., as a member of research staff. In 1994, he was a Research Fellow with the British Telecom Labs, Martlesham, U.K., and then in 1995 joined, as a Faculty, the Department of Electrical Engineering and Electronics, University of Liverpool, Liverpool, U.K., where he is currently a Full Professor in Wireless Engineering, the Head of High-Frequency Engineering Group, and Deputy Head of Department. He has authored more than 350 refereed papers in leading international journals and conference proceedings, and authored *Antennas: From Theory to Practice* (Wiley, 2008) and *Reverberation Chambers: Theory and Applications to EMC and Antenna Measurements* (Wiley, 2016). Since 1987, he has been conducting research in the areas of wireless communications, applied electromagnetics, radar, and antennas.

Prof. Huang has received many research grants from research councils, government agencies, charity, EU, and industry, acted as a consultant to various companies, and served on a number of national and international technical committees and has been an Editor, Associate Editor, or Guest Editor for five international journals. He has been a keynote/invited speaker and organizer of many conferences and workshops (e.g., International Conference on Wireless Communications, Networking and Mobile Computing 2006 and 2010, IEEE International Workshop on Antenna Technology 2010, Loughborough Antennas and Propagation Conference 2012, and European Conference on Antennas and Propagation 2018). He is currently the Editor-in-Chief for *Wireless Engineering and Technology*, Associate Editor for the IEEE ANTENNAS AND WIRELESS PROPAGATION LETTERS, U.K. and Ireland Rep to European Association of Antenna and Propagation, a Fellow of IET, and a Senior Fellow of HEA.